Energy Proceedings
Vol 36, 2023
ISSN 2004-2965

Enabling Unlabelled Field Data for Battery Health Diagnosis by Decoupling Experiment

Qiushi Wang[1,2], Zhenpo Wang[1,2,3], Peng Liu[1,2,3], Yiwen Zhao[1,2], Ni Lin[1,2*]

1 National Engineering Research Center of Electric Vehicles, Beijing Institute of Technology, Beijing 100081, China

2 Beijing Co-innovation Center for Electric Vehicles, Beijing 100081, China.

3 Beijing Institute of Technology Chongqing Innovation Center, Chongqing 401120, China

(*Corresponding Author: 6120200190@bit.edu.cn)

ABSTRACT

There is a rising need for accurate battery state of health (SOH) diagnosis in electric vehicle maintenance and second-life evaluation. However, existing methods suffer from the transition from cell-level tests to real-world vehicle applications due to the ignorance of incorporating laboratory tests with large-scale, time-varying field data. This paper proposes a framework combining the system-level capacity calculation and cell-level decoupling experiment for battery system capacity diagnosis. A modified regional capacity calculation method for online applications is presented, and the regional capacity of the battery under various temperatures and SOHs is experimentally determined to decouple various working conditions. This work highlights the opportunity to integrate laboratory test data to leverage unlabelled field data for capacity diagnosis while revealing the characteristics of battery capacity under different working conditions.

Keywords: Lithium-ion batteries, electric vehicles, health diagnosis, field data, decoupling experiment

NOMENCLATURE

Abbreviations	
EV	Electric vehicle
SOH	State of health
EM	Electrochemical model
ECM	Equivalent circuit model
IC	Incremental capacity
CC	Constant current
CV	Constant voltage
OCV	Open circuit voltage
SOC	State of charge
L-M	Levenberg-Marquardt
MAPE	Mean absolute percentage error
RMSE	Root mean squared error

1. INTRODUCTION

Rapid decarbonization of the transportation sector is an important but challenging demand for carbon neutrality pledges [1]. The transition to electric vehicles (EVs) is a viable way to decrease the carbon footprint of passenger cars in cities [2]. As the leading energy storage component of EVs, Lithium-ion batteries have gained wide attention in academic research and industrial applications [3]. However, batteries undergo inevitable degradation in terms of capacity and internal resistance due to the time-varying working conditions, this poses a great challenge for battery state of health (SOH) diagnosis [4].

Various approaches have been proposed in the literature to realize battery health diagnosis and estimation, which can be divided into either model-based methods or data-driven methods [5]. Model-based methods use mathematical equations or physics-based model equations to describe battery dynamics and degradation behaviour [6]. Electrochemical models (EMs) and equivalent circuit models (ECMs) are widely used models. EMs use partial differential equations to depict battery degradation mechanisms like the loss of lithium inventory, the loss of active material in the electrodes, and the increase of internal resistance [7]. EMs can reach satisfying estimation accuracy, however, the computational complexity hinders their application [8]. Apart from that, ECMs are ubiquitously used for battery ageing modelling, they use circuitry elements to simulate the dynamic characteristics of the battery [9]. Bayesian filtering techniques and adaptive observers are commonly used for predicting the evolution of the parameters [10,11]. The ECM-based methods can achieve multi-parameter joint estimation, but the generalization ability is not satisfied.

In contrast, data-driven methods use statistical theories or machine learning techniques to build models

This is a paper for the 9th Applied Energy Symposium: Low Carbon Cities and Urban Energy Systems (CUE2023), Sep. 2-7, 2023, Matsue & Tokyo, Japan.

to delineate the relationship between the features and the prediction targets [12], they have no requirements for detailed knowledge about chemical and electrochemical reactions underlying the battery. Multiple battery ageing features can be derived from the historical monitoring data of batteries through incremental capacity (IC) analysis, differential voltage analysis and differential thermal voltammetry [13–15]. The ageing features are trained by various kinds of machine learning-based algorithms such as support vector regression, artificial neural network, Gaussian process regression, long short-term memory recurrent neural network [16,17].

However, the existing methods either focus on controlled laboratory tests or barely EV field data. The results of laboratory tests lack the ability to fit the time-varying, uncontrolled real-world scenarios, and the models are only trained on cell-level data. On the contrary, the results of field data-based methods are coupled with working conditions such as temperature, so the data labels (full discharge capacity under standard conditions) are missing. Therefore, it is vital to associate the cell-level laboratory test with system-level EV battery field data.

To tackle the aforementioned issue, this paper proposed a health diagnosis framework for real-world electric buses that combines field data-based battery system capacity calculation and laboratory data-based cell-level capacity decoupling. The regional charging capacity is calculated in the field, and battery standard capacity under different temperatures, SOHs are measured by experiments to decouple capacity with temperature.

2. EXPERIMENT & DATA COLLECTION

2.1 Real-world EV dataset

The real-world dataset used in this study is collected from the open lab of the National Big Data Alliance for New Energy Vehicles. According to the data transmission protocol, 73 data items including general vehicle states (such as velocity, position, accumulated mileage), subsystem data(such as battery system voltage, current, SOC, motor power), fault alarm (over-voltage, nan value, inconsistency fault), etc., are transmitted to the platform in real-time at a sampling frequency of 0.1Hz [18]. Data of a type of electric buses are used in this study, the specifications are listed below.

TABLE I Specifications of the studied vehicle

Parameter	Value (Units)
Curb weight	8270 kg
Battery material	$LiFePO_4$ / Graphite
Battery pack capacity	240 Ah
Nominal voltage	537.6 V
Driving range	300 km
Pack configuration	2p168s

2.2 Battery capacity decoupling experiment

The experimental part aims at discovering the correlation between battery partial charging capacity, complete discharging capacity, and temperature. To this end, the experiment platform is built as shown in Fig. 1, where a four-channel battery tester (Arbin BT2000), a thermal chamber, testing batteries, and a host computer are included. The tester is used to provide current load of the predefined profile, and the voltage, temperature, charge/discharge capacity is recorded by the host computer. The tested batteries are 6 Ah 32700 cylindrical cells with $LiFePO_4$ / Graphite chemistry. The thermal chamber is used to control the environmental temperature of the batteries, and thermal couples are attached to the surface of the batteries to measure the temperature.

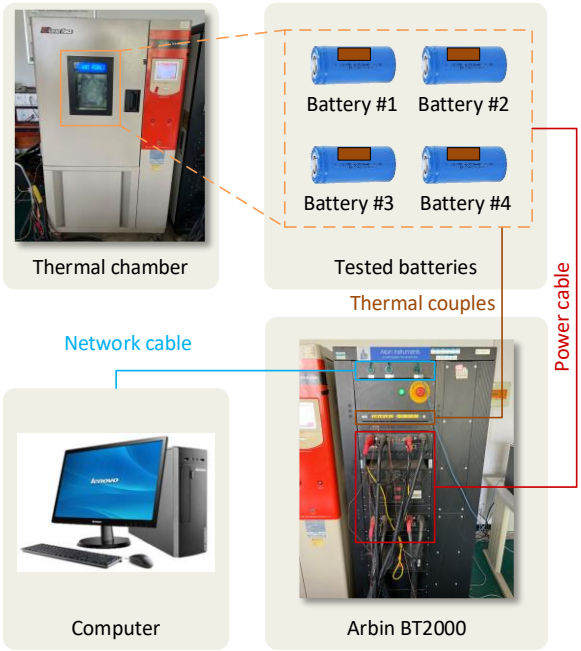

Fig. 1 Experiment setup

The overall experimental procedure can be described in Fig. 2, which has the following main steps:

1) Pretreatment: Pre-cycling is applied to each cell to activate and assess its performance. The cells were discharged to the cut-off voltage (2.0V) using 0.5C constant current (CC) and then rested for 30 minutes. Next, the cells were charged with a constant current-constant voltage (CC-CV) charging mode (0.5C at the CC stage to 3.65V, then CV until the current dropped to 0.05C). After another 30-minute rest, this discharge and charge process was repeated three times.

2) Standard capacity test: This serves as the capacity calibration under various temperatures. Since the tested cells have different initial SOCs, they are firstly discharged to the cut-off voltage using 0.5C current. After 30-minute rest, the cells are charged with the CC-CV profile which is the same as the pretreatment cycles. Then, rest for 30 minutes, and the cells are discharged at 0.5C to the cut-off voltage. The current load and voltage response is shown in Fig. 3.

3) Accelerated ageing test: If the capacity of the cell is not at the predefined SOH level, accelerated ageing test are used to adjust. The cells are charged with a CC-CV profile (3C until 4.5 V, then change to CV step until the current drop to 0.05C), rest for 5 minutes, followed by a CC discharge step with 3C until the voltage drop to 1.8 V.

Ten fresh cells and 80 aged cells with different SOHs are collected. We measured the charge and discharge curves at six different SOH levels (100%, 95%, 93%, 90%, 87%, 85%) and six different ambient temperatures (-2 °C, 5 °C, 15 °C, 25 °C, 35 °C, 45 °C), which made a 6×6 grid. For each cell, pretreatment is conducted first. After the standard capacity test for all the cells, we chose several cells that have the most similar capacity to the predefined SOH levels. Accelerated ageing tests are applied if the capacity is not exactly the requested. Then, standard capacity tests are utilized at each temperature level.

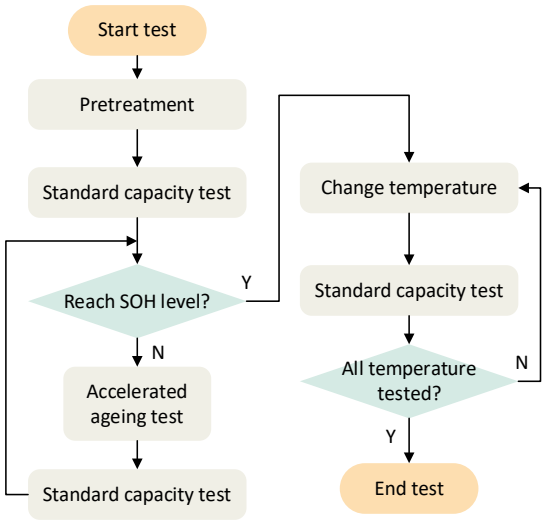

Fig. 2 Experiment procedure

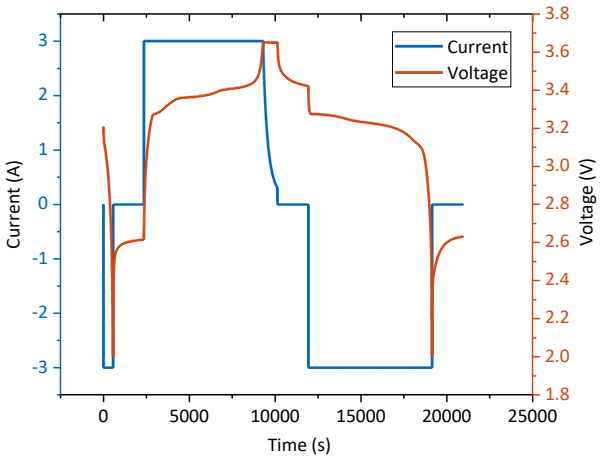

Fig. 3 Standard capacity test load profile and voltage response

3. METHODOLOGY

The overall framework of the proposed battery system SOH diagnosis method is illustrated in Fig. 4, which consists of three main parts: system-level capacity calculation, cell-level decoupling test, and battery system SOH diagnosis. For the first part, field dataset of electric buses is used, after data pre-processing and transformation, qualified charging segments are collected. Combining Coulomb counting and IC analysis, the modified regional capacity is calculated using battery system field data. For cell-level decoupling test, we test battery charging/discharging capacity under different temperatures and SOHs, then a three-dimensional responding surface is drawn. Finally, for the SOH diagnosis part, the voltage interval and regional capacity for battery system is converted into cell scale, and quadratic equation solving is implemented to map the regional capacity into battery SOH under standard conditions.

3.1 Modified regional capacity calculation

Regional charging capacity is demonstrated to be an effective battery health indicator and is linearly correlated with the full capacity under standard conditions [19,20]. The calculation method of regional capacity is shown as follows:

$$C_r(\tau) = \int_{t(V_1)}^{t(V_2)} I(t)\,dt \tag{1}$$

$$V_1 = V_{peak} - \Delta V_{\text{int}} / 2 \tag{2}$$

$$V_2 = V_{peak} + \Delta V_{\text{int}} / 2 \tag{3}$$

where C_r denotes the regional capacity, $I(t)$ represents the current at time t, $t(V_1)$ and $t(V_2)$ are the start and end time for the regional battery capacity

calculation of the voltage interval $\Delta V_{\text{int}} = [V_1, V_2]$, and V_{peak} is the terminal voltage corresponding to the IC peak.

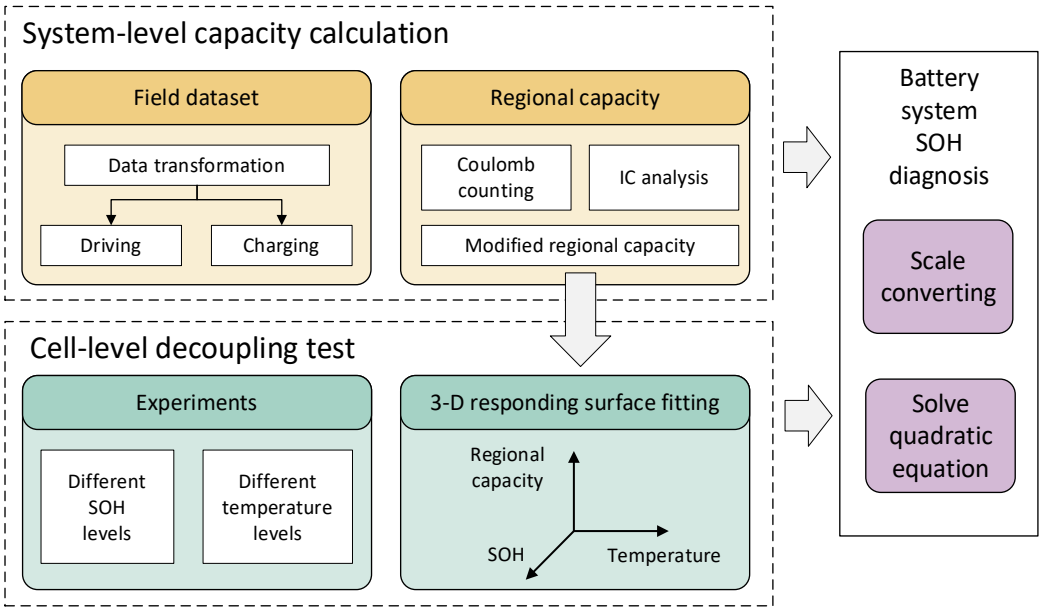

Fig. 4 Framework of the proposed battery system SOH diagnosis method

However, the regional capacity in existing methods is usually calculated under fixed temperature and low current rates. In such cases, the corresponding open circuit voltage (OCV) range is also fixed, ensuring a linear relationship between the regional capacity and the overall battery capacity. But in real-world electric vehicle applications, different charging instances involve varying temperatures and charging currents, so the IC curves will shift from left to right due to the decrease of temperature, as illustrated in Fig. 5. This makes the fixed-interval regional capacity method invalid.

Hence, we developed a modified regional capacity calculation method with moving voltage intervals, which is suitable for electric vehicle battery packs operating under complex and varying conditions, defined by $C_r'(\tau)$:

$$C_r'(\tau) = \int_{t(V_1')}^{t(V_2')} I(t)\,dt \tag{4}$$

where V_1' and V_2' are the start and end voltages around the IC peak region.

The determination of the voltage interval position and length is based on the usage behaviour of the studied battery. From statistical analysis, we found that the charging voltage is mostly between 560 V and 572 V, and the position of the second IC peak is located around 569 V [18]. Therefore, we set [560 V, 572 V] as the base interval, and the actual interval of each charging curve is calculated by the difference between the second IC peak position and 569 V. The final voltage inteval is defined as $\Delta V = [V_1',\ V_2'] = 12\text{V}$, with

$$V_1' = 560 + (V_{peakB} - 569) \tag{5}$$

$$V_2' = 572 + (V_{peakB} - 569) \tag{6}$$

Two exampled IC curves and their corresponding voltage intervals are shown in Fig. 5.

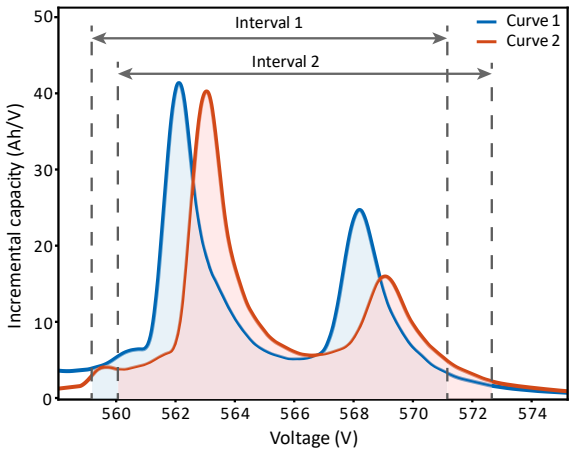

Fig. 5 Diagram of the modified regional capacity method

3.2 Three-dimensional responding surface fitting

Having the system-level voltage interval for regional capacity calculation determined, it is necessary to convert system-level data to cell-level, so that the decoupling experiment can be implemented. Since the battery pack has a 168-serial configuration, the 12 V voltage length (ΔV) is equal to 0.0714 V in cell-level. When transitioning the regional capacity, considering the nominal capacity of the battery system is 240 Ah, and the nominal capacity of the tested battery cell is 6 Ah, we can convert the system-level regional capacity C_r' to cell-level $C_{r,cell}'$ as:

$$C_{r,cell}' = \frac{C_r'}{240} \times 6 \tag{7}$$

After converting the calculated battery system regional capacity in EV in real-time to a cell-level regional capacity, we should map this value to battery discharge capacity at standard discharging rate and temperature, i.e., SOH, which is the purpose of the decoupling experiment illustrated in Section 2.2. Therefore, a three-dimensional responding surface fitting method is needed to establish the relationship between temperature, SOH, and regional capacity, and further map the regional capacity to standard SOH. Here, quadratic polynomial fitting is implemented, which will fit the three-dimensional surface as the following equation:

$$z = z0 + ax + by + cx^2 + dy^2 + fxy \tag{8}$$

where *x*, *y*, and *z* are three axes, and *z*0, *a*, *b*, *c*, *d*, and *f* are model parameters to be identified.

Levenberg-Marquardt (L-M) algorithm is applied in this study to identify the parameters. The L-M algorithm stands out as a highly efficient technique for fitting parameters in nonlinear models [21]. Combining the rapid convergence characteristics of the Gauss-Newton steepest descent method with the adaptive capabilities of a neural network, the L-M algorithm demonstrates exceptional performance in model parameter estimation.

4. RESULTS & DISCUSSION

4.1 Comparison of capacities under different conditions

The capacities under different SOHs and temperatures are shown in Fig. 6. It can be seen that the regional charging capacity decreases with decreasing temperature at every SOH level. It is worth noted that the capacity difference between various SOHs at 45 °C is 1.15 Ah, but only 0.24 Ah at -2 °C, indicating that under low temperatures, the available capacities of both fresh and aged cells are low. On the other side, for the cell with 100% SOH, the capacity difference between 45 °C and -2 °C is 1.5 Ah, and for the cell with 85% SOH, the difference is only 0.57 Ah, indicating that the effect of temperature on the capacity of fresh cells is greater than that of aged ones.

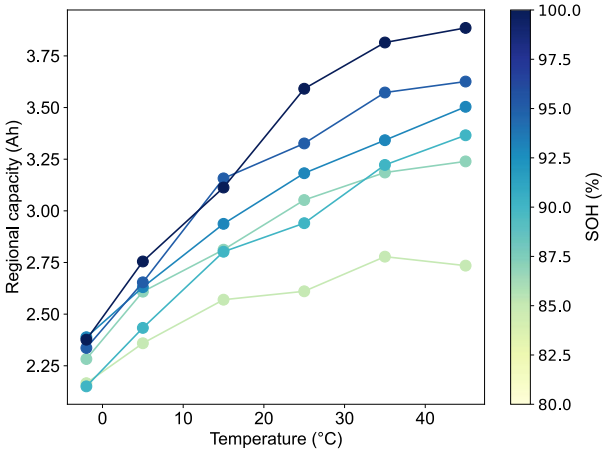

Fig. 6 Regional capacity at different temperatures and SOHs.

4.2 Decoupled battery capacity analysis

The fitted three-dimensional capacity responding surface is shown in Fig. 7. Using the polynomial equation given by Eq. (8), the surface fitting is accurate with an R-square (R^2) value of 96%. Through L-M parameter identification, the parameters of Eq. (8) is determined, denote SOH as *S*, temperature as *T*, the final equation of the responding surface can be written as Eq. (9).

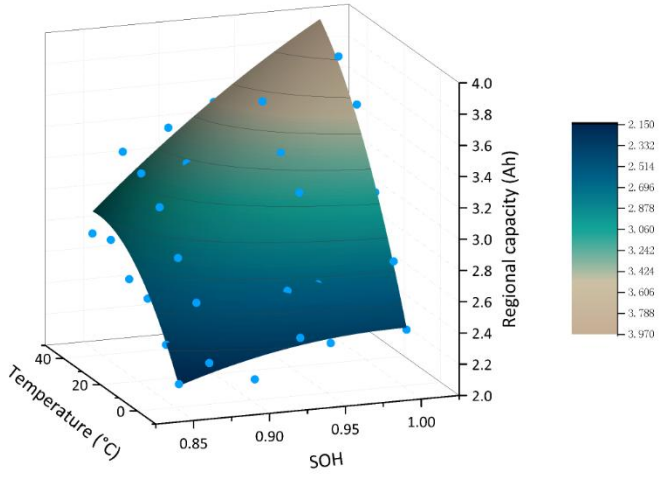

Fig. 7 Three-dimensional capacity responding surface

$$C_{r,cell}' = -8.62 + 22.05S - 0.07T - 10.94S^2 - 3.82\times10^{-4}T^2 + 0.12ST \tag{9}$$

Fitting errors are illustrated in Fig. 8. The fitted capacity is linearly correlated to the measured capacity

of the test, which means the fitting result is accurate. The mean absolute percentage error (MAPE) and the root mean squared error (RMSE) are used as metrics of the fitting results. The MAPE of all the 36 points is 2.56 %, and the RMSE is 0.095 Ah, which further validated the fitting accuracy.

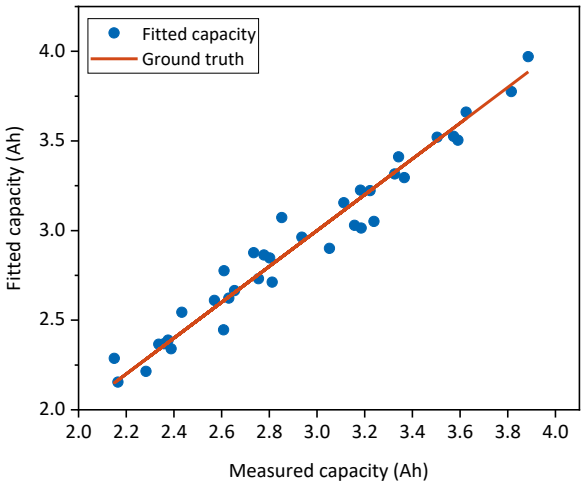

Fig. 8 Error analysis of the surface fitting

Based on the Three-dimensional capacity responding surface and Eq. (9), we can map the regional capacity under various temperatures into standard battery SOH. Eq. (9) can be transformed into a general quadratic equation form as

$$10.94S^2-\left(0.12T+22.05\right)S+\left(C'_{r,cell}+3.82\times10^{-4}T^2+0.07T+8.62\right)=0 \quad (10)$$

Given $C'_{r,cell}$ and T, the battery SOH can be calculated by Eq. (10) and the quadratic equation root formula.

Based on the mentioned procedure, Table II displays sample results for the diagnosis of battery system SOH. The data illustrates how the regional charging capacity of the battery system can be reliably mapped to the battery's SOH under standard conditions, thus confirming the efficacy of the proposed framework.

TABLE II SOH diagnosis results

Test No.	Regional cap. (Ah)	Temp. (°C)	SOH (%)
1	149.6	39.6	97.5
2	136.8	29.5	95.0
3	126.2	35.8	88.8
4	121.9	33.1	87.6
5	112.1	32.8	84.3

5. CONCLUSIONS

Integrating real-world EV battery system capacity calculation with laboratory-based experimental tests is an important but challenging way to realise battery system SOH diagnosis. To tackle this issue, this paper presents a battery SOH diagnosis framework combining system-level regional capacity calculation and cell-level capacity decoupling test. At system-level, a regional capacity calculation method with moving voltage intervals is designed based on Coulomb counting and incremental capacity analysis. At cell-level, battery cell charging and discharging capacities under different temperatures are experimentally measured. To integrate these two parts, an equivalent scale converting method is proposed from battery system to battery cell, and battery SOH under standard working conditions are derived by three-dimensional responding surface mapping. The results show that the capacity responding surface is fitted accurately, and the battery SOH can be effectively calculated by the proposed method. This study presents a feasible approach to bridge the gap between laboratory tests and electric vehicle field application. This method can be widely applied in battery health management, second-life evaluation, and maintenance scheduling.

ACKNOWLEDGEMENT

This work is supported by Ni Lin's Overseas High-level Talent Introduction Program - Youth Project (Grant number: 3030022212208).

REFERENCE

[1] Chen W, Sun X, Liu L, Liu X, Zhang R, Zhang S, et al. Carbon neutrality of China's passenger car sector requires coordinated short-term behavioral changes and long-term technological solutions. One Earth 2022;5:875–91. https://doi.org/10.1016/j.oneear.2022.07.005.

[2] Morfeldt J, Johansson DJA. Impacts of shared mobility on vehicle lifetimes and on the carbon footprint of electric vehicles. Nat Commun 2022;13:6400. https://doi.org/10.1038/s41467-022-33666-2.

[3] Che Y, Stroe D-I, Sui X, Vilsen SB, Hu X, Teodorescu R. Battery Aging Behavior Evaluation Under Variable and Constant Temperatures with Real Loading Profiles. 2023 IEEE Applied Power Electronics Conference and Exposition (APEC), Orlando, FL, USA: IEEE; 2023, p. 2979–83. https://doi.org/10.1109/APEC43580.2023.10131534.

[4] Gasper P, Schiek A, Smith K, Shimonishi Y, Yoshida S. Predicting battery capacity from impedance at varying temperature and state of charge using machine learning. Cell Reports Physical Science 2022;3:101184. https://doi.org/10.1016/j.xcrp.2022.101184.
[5] Li W, Zhang H, van Vlijmen B, Dechent P, Sauer DU. Forecasting battery capacity and power degradation with multi-task learning. Energy Storage Materials 2022;53:453–66.
https://doi.org/10.1016/j.ensm.2022.09.013.
[6] Hu X, Xu L, Lin X, Pecht M. Battery Lifetime Prognostics. Joule 2020;4:310–46. https://doi.org/10.1016/j.joule.2019.11.018.
[7] Marcicki J, Canova M, Conlisk AT, Rizzoni G. Design and parametrization analysis of a reduced-order electrochemical model of graphite/LiFePO4 cells for SOC/SOH estimation. Journal of Power Sources 2013;237:310–24.
https://doi.org/10.1016/j.jpowsour.2012.12.120.
[8] Zhou L, Zhao Y, Li D, Wang Z. State-of-Health Estimation for LiFePO $_4$ Battery System on Real-World Electric Vehicles Considering Aging Stage. IEEE Trans Transp Electrific 2022;8:1724–33. https://doi.org/10.1109/TTE.2021.3129497.
[9] Zhang X, Wang Y, Liu C, Chen Z. A novel approach of battery pack state of health estimation using artificial intelligence optimization algorithm. Journal of Power Sources 2018;376:191–9. https://doi.org/10.1016/j.jpowsour.2017.11.068.
[10] Chen C, Xiong R, Shen W. A Lithium-Ion Battery-in-the-Loop Approach to Test and Validate Multiscale Dual H Infinity Filters for State-of-Charge and Capacity Estimation. IEEE Trans Power Electron 2018;33:332–42. https://doi.org/10.1109/TPEL.2017.2670081.
[11] Xiong R, Zhang Y, He H, Zhou X, Pecht MG. A Double-Scale, Particle-Filtering, Energy State Prediction Algorithm for Lithium-Ion Batteries. IEEE Trans Ind Electron 2018;65:1526–38. https://doi.org/10.1109/TIE.2017.2733475.
[12] Liu K, Shang Y, Ouyang Q, Widanage WD. A Data-Driven Approach With Uncertainty Quantification for Predicting Future Capacities and Remaining Useful Life of Lithium-ion Battery. IEEE Trans Ind Electron 2021;68:3170–80.
https://doi.org/10.1109/TIE.2020.2973876.
[13] Dubarry M, Liaw BY, Chen M-S, Chyan S-S, Han K-C, Sie W-T, et al. Identifying battery aging mechanisms in large format Li ion cells. Journal of Power Sources 2011;196:3420–5.
https://doi.org/10.1016/j.jpowsour.2010.07.029.
[14] Wang L, Pan C, Liu L, Cheng Y, Zhao X. On-board state of health estimation of LiFePO4 battery pack through differential voltage analysis. Applied Energy 2016;168:465–72.
https://doi.org/10.1016/j.apenergy.2016.01.125.
[15] Wu B, Yufit V, Merla Y, Martinez-Botas RF, Brandon NP, Offer GJ. Differential thermal voltammetry for tracking of degradation in lithium-ion batteries. Journal of Power Sources 2015;273:495–501. https://doi.org/10.1016/j.jpowsour.2014.09.127.
[16] Klass V, Behm M, Lindbergh G. A support vector machine-based state-of-health estimation method for lithium-ion batteries under electric vehicle operation. Journal of Power Sources 2014;270:262–72. https://doi.org/10.1016/j.jpowsour.2014.07.116.
[17] Ren L, Dong J, Wang X, Meng Z, Zhao L, Deen MJ. A Data-Driven Auto-CNN-LSTM Prediction Model for Lithium-Ion Battery Remaining Useful Life. IEEE Trans Ind Inf 2021;17:3478–87. https://doi.org/10.1109/TII.2020.3008223.
[18] Wang Q, Wang Z, Zhang L, Liu P, Zhou L. A Battery Capacity Estimation Framework Combining Hybrid Deep Neural Network and Regional Capacity Calculation Based on Real-World Operating Data. IEEE Trans Ind Electron 2023;70:8499–508.
https://doi.org/10.1109/TIE.2022.3229350.
[19] Tang X, Zou C, Yao K, Chen G, Liu B, He Z, et al. A fast estimation algorithm for lithium-ion battery state of health. Journal of Power Sources 2018;396:453–8. https://doi.org/10.1016/j.jpowsour.2018.06.036.
[20] Huang S, Liu C, Sun H, Liao Q. State of health estimation of lithium-ion batteries based on the regional frequency. Journal of Power Sources 2022;518:230773. https://doi.org/10.1016/j.jpowsour.2021.230773.
[21] Zhang C, Jiang Y, Jiang J, Cheng G, Diao W, Zhang W. Study on battery pack consistency evolutions and equilibrium diagnosis for serial- connected lithium-ion batteries. Applied Energy 2017;207:510–9. https://doi.org/10.1016/j.apenergy.2017.05.176.